



HAL
open science

TEM EDS analysis of epitaxially-grown self-assembled indium islands

Jasmine Sears, Ricky Gibson, Michael Gehl, Sander Zandbergen, Patrick Keiffer, Nima Nader, Joshua Hendrickson, Alexandre Arnoult, Galina Khitrova

► **To cite this version:**

Jasmine Sears, Ricky Gibson, Michael Gehl, Sander Zandbergen, Patrick Keiffer, et al.. TEM EDS analysis of epitaxially-grown self-assembled indium islands. AIP Advances, 2017, 7 (5), 10.1063/1.4983492 . hal-01912407

HAL Id: hal-01912407

<https://hal.science/hal-01912407>

Submitted on 5 Nov 2018

HAL is a multi-disciplinary open access archive for the deposit and dissemination of scientific research documents, whether they are published or not. The documents may come from teaching and research institutions in France or abroad, or from public or private research centers.

L'archive ouverte pluridisciplinaire **HAL**, est destinée au dépôt et à la diffusion de documents scientifiques de niveau recherche, publiés ou non, émanant des établissements d'enseignement et de recherche français ou étrangers, des laboratoires publics ou privés.

TEM EDS Analysis of Epitaxially-Grown Self-Assembled Indium Islands

Jasmine Sears, Ricky Gibson, Michael Gehl, Sander Zandbergen, Patrick Keiffer, Nima Nader, Joshua Hendrickson, Alexandre Arnoult, Galina Khitrova

Abstract

Epitaxially-grown self-assembled indium nanostructures, or islands, show promise as nanoantennas. The elemental composition and internal structure of indium islands grown on gallium arsenide are explored using Transmission Electron Microscopy (TEM) Energy Dispersive Spectroscopy (EDS). Several sizes of islands are examined, with larger islands exhibiting high (>94%) average indium purity and smaller islands containing inhomogeneous gallium and arsenic contamination. These results enable more accurate predictions of indium nanoantenna behavior as a function of growth parameters.

1. Background

As the field of plasmonic nanostructures develops, there is increasing demand for epitaxially-grown metallic nanostructures. Metal-on-semiconductor nanoantennas, which operate at optical and near-infrared wavelengths, have a wide range of potential applications, from low-cost photodetectors¹ to higher-efficiency solar cells.² Currently, nanoantenna fabrication is often performed separately from substrate preparation;^{3–8} this discontinuity can adversely affect the finished product through contamination and impurities introduced during fabrication. One method for avoiding these issues is to epitaxially grow both the substrate and plasmonic nanostructure, with the structure self-assembling from a uniformly-deposited metal layer such as silver or indium.^{9,10} Self-assembled nanostructures can additionally benefit from a better contact interface between structure and substrate compared to other fabrication methods. Epitaxially-grown nanostructures may also have applications in quantum computing.^{11,12} Majorana fermions, a candidate for qubit construction, have been observed in InSb nanowires coupled to superconducting NbTiN.¹³ Other s-wave superconductor-1D semiconductor systems are also expected to generate Majorana fermions; InAs and indium have been identified as a potential semiconductor and superconductor, respectively.^{14,15} InAs nanowires can be grown epitaxially, suggesting that self-assembled indium islands may allow for the epitaxial growth of entire Majorana fermion-generating heterostructures.

While epitaxially-grown self-assembled indium islands show promise as nanoantennas,¹⁶ the internal structure of these islands has not been thoroughly explored. Prior work has indicated that these structures may contain impurities unique to the epitaxial growth process.¹⁷ This paper seeks to describe and analyze the internal structure of indium islands grown under three different sets of growth conditions, in order to better predict the behavior and future applications of these plasmonic nanostructures.

2. Experiment

The indium islands analyzed in this work were grown via Molecular Beam Epitaxy (MBE), using the equipment and procedures described in Ref. 17. The growth parameters of each sample are listed in Table I. Three samples, shown in Fig. 1, are discussed: a sample with islands averaging 125nm in diameter (In38), a sample with islands averaging 1.5 μ m in diameter (In44), and a sample with islands averaging 2.5 μ m in diameter (In54). All three samples were grown on GaAs substrates, and In38 contained an InGaAs quantum well 5nm below the surface of the substrate. For each sample, after completion of the substrate growth, the substrate was allowed to cool to a stable temperature and residual arsenic was pumped from the growth chamber before the deposition of indium.

Table 1. Sample growth parameters.

| Sample | Substrate temp. (°C) | Indium temp. (°C) | Arsenic clear time (hours) | Deposition rate | Monolayers of indium |
|--------|----------------------|-------------------|----------------------------|-----------------|----------------------|
| In38 | 133 | 830 | 1.3 | 0.543 ML/sec | 12 |
| In44 | 131 | 510 | 12 | 1 ML/hour | 12 |
| In54 | 131 | 510 | 12 | 1 ML/hour | 36 |

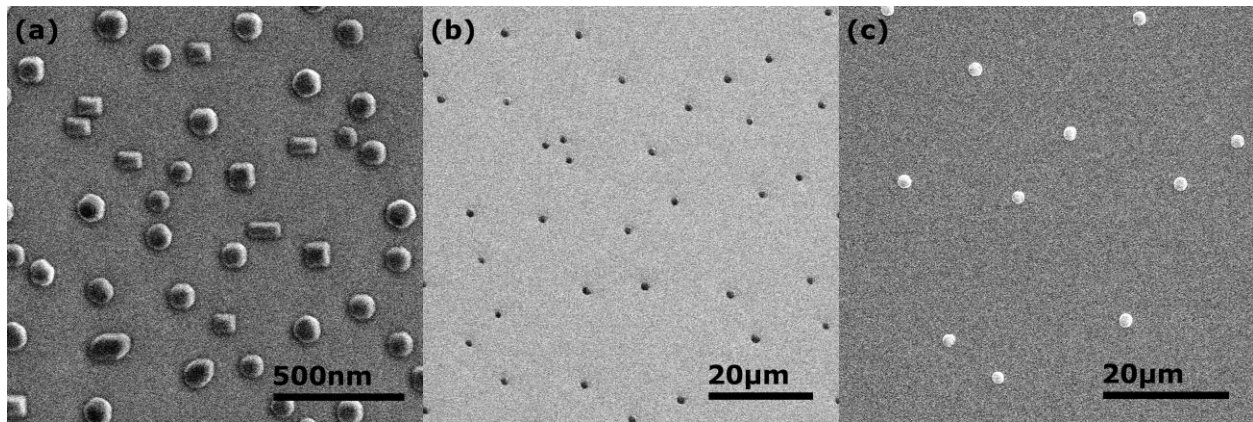


Fig. 1. SEM images of indium island samples In38 (a), In44 (b), and In54 (c).

In order to determine the spatially-dependent composition of the islands, a combination of Transmission Electron Microscopy (TEM) and Energy Dispersive Spectroscopy (EDS) was used. Thin cross-sections of each sample were analyzed by focusing a narrow electron beam on the sample and collecting the resulting x-ray spectrum. Each of the elements of interest have distinct x-ray emission spectra, as shown in Fig. 2, allowing qualitative maps of island composition to be constructed by collecting x-ray spectra from an array of points.

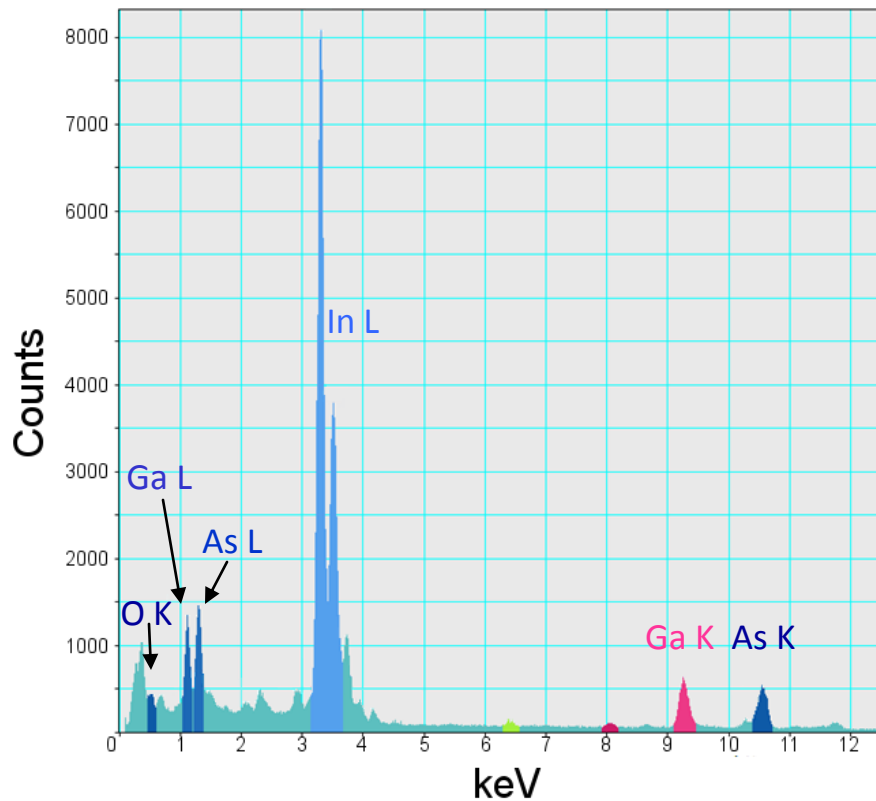


Fig. 2. An x-ray emission spectrum from In38. The peaks of each of the elements of interest (O, Ga, As, In) are highlighted to show that the In, Ga, and As lines do not overlap.

The analysis of the In38 islands was performed using a JEOL 2010F TEM with an EDAX-manufactured 30mm² atmospheric thin window SiLi EDX detector. A JEOL ARM200F with a JEOL-manufactured 50mm² windowless SiLi EDX detector was used to analyze the In44 and In54 islands. The resolution of the EDS area maps and line scans ranges from 1.4nm to 4nm. Quantitative EDS, measuring the average atomic percentage composition of a region, was performed by expanding the beam to cover a large area of the In38 and In44 islands, and by measuring an array of points on the In54 island. The measured area was approximately 10% of each of the In38 islands, 17% of the In44 island, and 3% of the In54 island. Quantitative EDS error estimates were obtained from the collection software and from calibration measurements.

To prepare the TEM cross-sections, the regions to be analyzed were covered in a protective coating composed of 10nm of electron beam-deposited carbon, followed by 500nm of electron beam-deposited platinum, and finally 2 μ m of ion beam platinum, with the electron beam-deposited layers serving to protect the surface of the sample from damage during the deposition of the ion beam platinum layer. A slab of material was then cut from the bulk sample using a focused gallium ion beam. The slab was gradually thinned using progressively weaker beam strengths, with the protective coating preventing damage to the underlying sample. Cross-sections were thinned to roughly 60nm (In38) or 100nm (In44, In54). Due to differences in island spacing and size constraints on cross-section preparation, three In38, two In44, and one In54 island were analyzed.

3. Results

A quantitative comparison of island centers, found in Table II, shows increasing indium purity with increasing island size. However, the islands were not homogenous; Fig. 3 shows EDS maps of the islands, and Fig. 4 shows annotated line scans of the In54 island and one In38 island. These images reveal several distinct features: all three of the examined In38 islands contained large regions of high gallium and arsenic and low indium concentrations; both of the examined In44 islands contained high gallium and arsenic and low indium concentrations at the island corners; and the In54 island exhibited a 50nm-tall arsenic-rich band along the base of the island.

Table 2. Elemental composition of island interiors by atomic percentage.

| Sample | In | Ga | As |
|--------|-------|-------|-------|
| In38 | 66.0% | 12.7% | 21.3% |
| | 89.9% | 5.6% | 4.5% |
| | 82.5% | 8.0% | 9.4% |
| In44 | 94.7% | 3.1% | 2.2% |
| In54 | 96.1% | 2.5% | 1.41% |

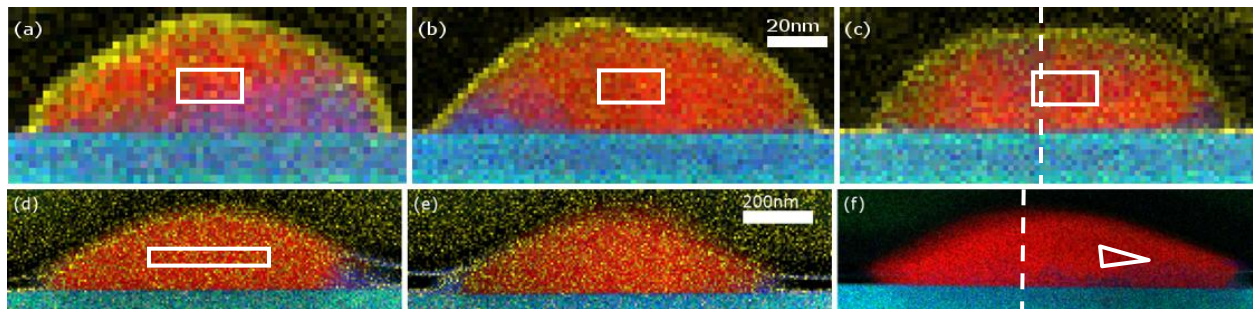


Fig. 3. False-color elemental composition maps of In38 (a, b, c), In44 (d, e), and In54 (f) islands. The white boxes show the approximate area over which quantitative EDS was performed, and the dashed lines show the line scan paths. The 20nm scale bar applies to a, b, and c, and the 200nm scale bar applies to d, e, and f. Red corresponds to In, blue to As, cyan to GaAs, purple to InGaAs, and yellow to O. Oxygen has been omitted from (f) to increase the visibility of As.

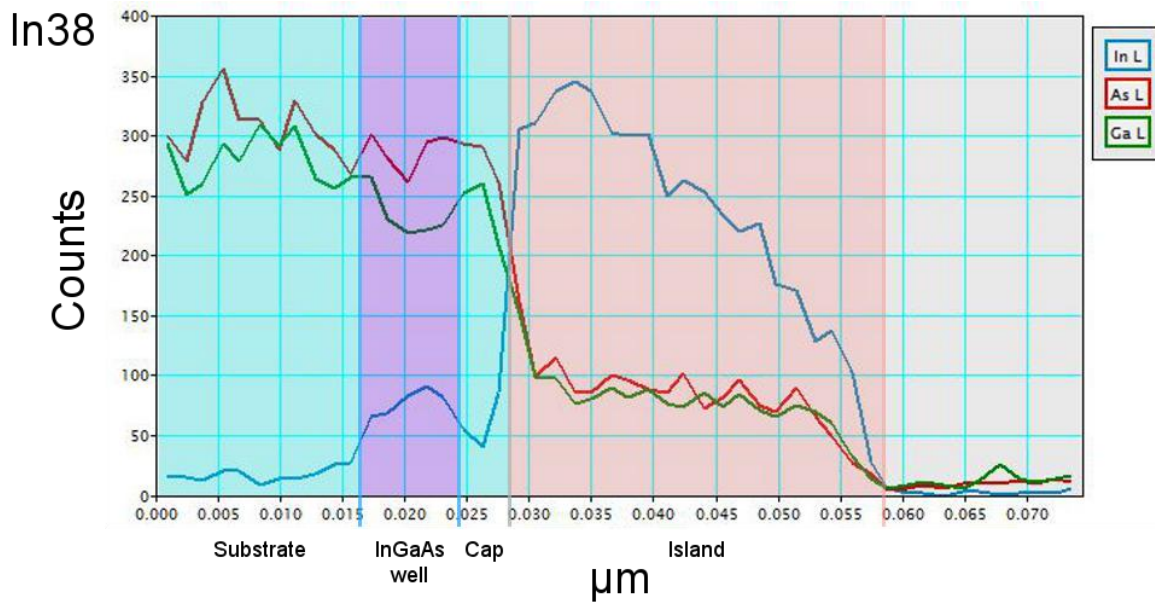
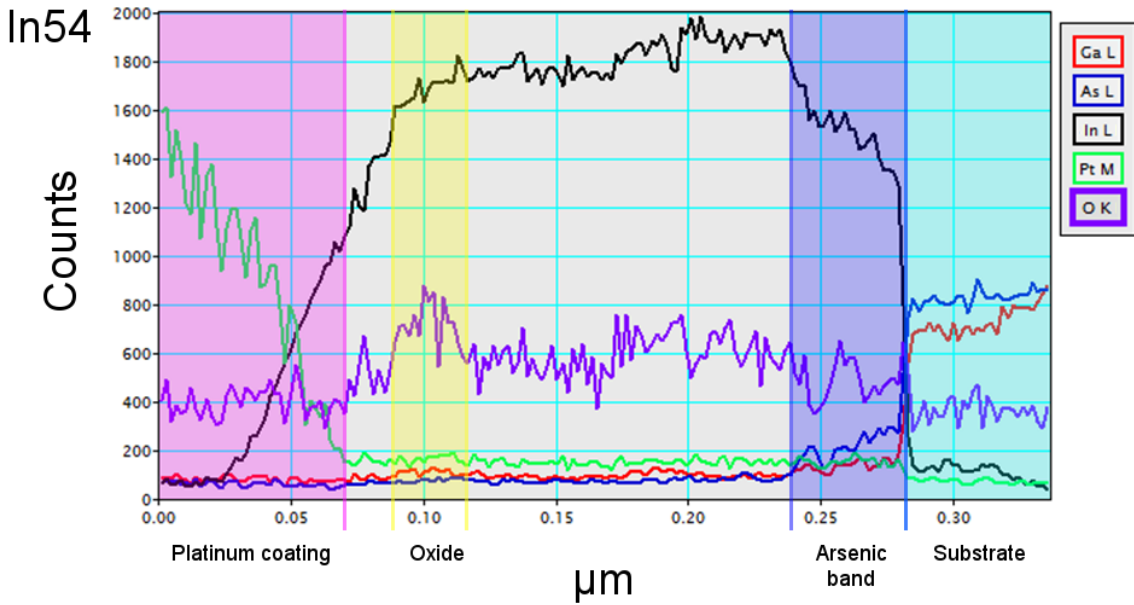


Fig. 4. Elemental composition line scans of In54 and In38, (f) and (c) in Fig. 3, with major regions highlighted. The line scan runs from above to below the In54 island and from below to above the In38 island. Lines are not normalized with respect to one another, but points along the same line can be qualitatively compared. The platinum coating has substantial overlap with the In54 island due to the TEM slice having non-negligible thickness compared to the curvature of the island.

Elemental composition line scans of In54 and In38, (f) and (c) in Fig. 3, with major regions highlighted. The line scan runs from above to below the In54 island and from below to above the In38 island. Lines are not normalized with respect to one another, but points along the same line can be qualitatively compared. The platinum coating has substantial overlap with the In54 island due to the TEM slice having non-negligible thickness compared to the curvature of the island.

All islands contained low concentrations of oxygen, with most islands exhibiting a distinct surface oxide. This surface oxide was approximately 4-7.5nm thick on In38, 15-25nm thick on In44, and 25nm thick on In54; the ratio of oxide thickness to island base diameter was roughly 1:20 for In38 and 1:100 for In44 and In54. All islands also contained an InGaAs region along the island-substrate interface. This region was roughly 5nm thick in In38 (b) and (c) and 10nm thick in the In44 and In54 islands. In38 (a) did not exhibit a sharp transition. This intermixed region was highly localized in most of the islands – the In54 substrate showed only 3.65% indium just 7nm below the island, and 0.66% indium 40nm below the island. Indium was also found in low concentrations in the GaAs cap layer separating the In38 islands from the InGaAs quantum well, as shown in Fig. 4b, although the InGaAs well remained distinct from the cap layer.

4. Discussion

The distribution of elements throughout the islands was not consistent between samples, suggesting that island properties or growth parameters may affect oxidation and intermixing between the substrate and islands. The high indium purities observed in the In44 and In54 islands indicate that superconducting behavior could be expected in these islands at low temperatures; superconductivity has been subsequently observed in In54.¹⁸ However, it seems unlikely that the In38 islands would exhibit superconducting behavior.

The oxygen signal from the islands was very noisy, due to the weak oxygen K line and its proximity to unrelated peaks. The differences in oxide layer thickness between the In44 and In54 islands can potentially be explained by measurement resolution, margins of error, and cross-section thickness, but the In38 island oxides appear significantly thinner. The In38 slices were thinner than the In44 and In54 slices, potentially giving a more accurate oxide thickness measurement. It is also possible that the higher concentrations of arsenic and gallium in the In38 islands impeded oxide growth, although the native oxides on both GaAs and pure indium tend to be roughly 4nm thick.^{19,20}

The inhomogeneous distribution of material within the In38 islands coupled with the smoothness of the GaAs substrate suggest that the semiconductor pockets within the islands precipitated from material that diffused into the indium during the initial deposition, before the material redistributed into islands. The indium temperature during the growth of In38 was 830°C, substantially higher than the temperature required to melt most In_{1-x}Ga_xAs alloys²¹ and similar to temperatures at which pronounced In-Ga intermixing has been observed.²²

Aside from different indium deposition temperatures, the arsenic pump-out time prior to growth was substantially shorter for In38 than for In44 or In54, which may have also contributed to the higher levels of arsenic found in the In38 islands. It is possible that the arsenic and gallium incorporated into the islands preferentially formed low-indium alloys which solidified while the rest of the island was still liquid, and which then combined into larger masses within the islands via Ostwald ripening.

In Fig. 1a, two island morphologies can be observed on In38: faceted islands, and rounded islands. Of the In38 islands examined, one (Fig. 3a) was faceted and two (Fig. 3b and c) were rounded. All three In38 islands exhibited substantial inhomogeneity; while the results suggest a possible relationship between In38 island morphology and composition, the number of characterized In38 islands is too small to draw meaningful conclusions.

The In44 and In54 island cross-sections showed arsenic and gallium contents that were lower on average and significantly more localized than in the In38 islands. The pattern of contamination at

the corners of the In₄₄ islands indicates the presence of a GaAs or InGaAs ring around the outer edge of the island, which may be similar to the InGaAs rings formed during GaAs capping of InAs quantum dots.²³ Although the length scales of the two systems are orders of magnitude different, it is possible that similar kinetic or thermodynamic forces are responsible for both; for example, the lattice constants of both InAs and crystalline indium are significantly greater than that of GaAs, suggesting that physical strain may play a similar role in quantum dot and larger island formation.

The arsenic-rich strip observed in In₅₄ (Fig. 4) is not mirrored in the other samples. Gallium is also present in this band, but in lower quantities, suggesting that diffusion of arsenic into indium is more energetically favorable than the diffusion of gallium into indium under In₅₄'s growth conditions. Simulations in the literature indicate that arsenic may have a longer diffusion length than gallium at the In₅₄ island-substrate interface temperature,²⁴ and arsenic is likely more mobile than gallium in pure indium due to the potential to form InAs rather than needing to fill indium vacancies.

The fairly-uniform horizontal distribution of arsenic and gallium in In₅₄, along with the decay in concentration with increasing distance from the base of the island, indicate that the materials diffused from the substrate after the indium along the interface had become relatively stationary. The arsenic and gallium concentrations in the In₃₈ islands do not show a similar decay with island height over distances similar to the height of the In₅₄ arsenic band, supporting the earlier remark that the presence of arsenic and gallium in the In₃₈ islands is likely not the result of diffusion post-island formation.

The observed patterns of intermixing suggest that low indium deposition temperatures are necessary for the formation of high-purity, homogeneous islands. In addition, shorter growth times may limit diffusion between the substrate and islands. The arsenic band along the base of the In₅₄ island and the arsenic- and gallium-rich rings around the In₄₄ islands seem unlikely to have a significant effect on nanoantenna behavior, but may impact the potential formation of Majorana fermions in islands coupled to InAs nanowires.

In summary, indium islands grown with low indium deposition temperatures exhibited high (>94%) indium purity throughout the main body of the island and highly-localized arsenic and gallium contamination. Low indium deposition temperature but longer deposition time resulted in very similar average indium purity, but the formation of a broad band of contamination along the island-substrate interface. Islands grown with high indium deposition temperatures contained large, irregular regions of gallium and arsenic contamination and a significantly lower (80%) average indium purity. The islands grown with a low indium deposition temperature were 1.5 μ m or larger in diameter, while the islands grown with a high indium deposition temperature were an average of 125nm in diameter. These results suggest that low indium deposition temperatures and short growth times contribute to the formation of high-purity, homogeneous islands. These results also suggest that superconducting behavior may be generally achievable in micron-scale islands, corresponding to mid-IR resonances. Modification of growth parameters may be necessary to produce self-assembled superconducting visible or near-IR nanoantenna arrays.

Acknowledgements

We gratefully acknowledge the use of facilities with the LeRoy Eyring Center for Solid State Science at Arizona State University. This work was funded by the Air Force Office of Scientific

Research (AFOSR, Dr. Gernot Pomrenke, Grant FA9550-13-1-0003), the National Science Foundation Atomic, Molecular and Optical Physics (NSF-AMOP 1205031) and the Engineering Research Center for Integrated Access Networks (NSF ERC-CIAN, Award EEC-0812072). JS would like to acknowledge the support of Arizona Technology and Research Initiative Funding (TRIF) and Professor Euan McLeod. MG would like to acknowledge the support of the Department of Defense through the National Defense Science and Engineering Graduate (NDSEG) Fellowship Program. SZ would like to acknowledge the support of the Department of Energy (DOE) through the Office of Science Graduate Fellowship (SCGF) made possible in part by the American Recovery and Reinvestment Act of 2009, administered by ORISE-ORAU under Contract no. DE-AC05-06OR23100. JH would like to acknowledge support from the Air Force Office of Scientific Research (AFOSR, Program Manager – Dr. Gernot Pomrenke, Contract 12RY05COR). AA would like to acknowledge support from the French technology network RENATECH.

References

- [1] Nazirzadeh, M. A., Atar, F. B., Turgut, B. B. & Okyay, A. K. Random sized plasmonic nanoantennas on Silicon for low-cost broad-band near-infrared photodetection. *Sci. Rep.* **4**, 7103 (2014).
- [2] Mokkaapati, S., Beck, F. J., de Waele, R., Polman, A. & Catchpole, K. R. Resonant nanoantennas for light trapping in plasmonic solar cells. *J. Phys. D: Appl. Phys.* **44**, 185101 (2011).
- [3] Klein, M. F. G. *et al.* Electron beam lithography of V-shaped silver nanoantennas. *Microelectron. Eng.* **86**, 1078–1080 (2009).
- [4] Kawakami, a., Saito, S. & Hyodo, M. Fabrication of nano-antennas for superconducting infrared detectors. *IEEE Trans. Appl. Supercond.* **21**, 632–635 (2011).
- [5] Chen, H., Bhuiya, A. M., Liu, R., Wasserman, D. M. & Toussaint, K. C. Design, Fabrication, and Characterization of Near-IR Gold Bowtie Nanoantenna Arrays. *J. Phys. Chem. C* **118**, 20553–20558 (2014).
- [6] Gadalla, M. N., Abdel-Rahman, M. & Shamim, A. Design, optimization and fabrication of a 28.3 THz nano-rectenna for infrared detection and rectification. *Sci. Rep.* **4**, 4270 (2014).
- [7] Gehl, M. *et al.* Spectroscopic studies of resonant coupling of silver optical antenna arrays to a near-surface quantum well. *J. Opt.* **16**, 114016 (2014).
- [8] Meinzer, N. *et al.* Arrays of Ag split-ring resonators coupled to InGaAs single-quantum-well gain. *Optics Express* **18** (23), 24140-24151 (2010).
- [9] Urbańczyk, A. & Nötzel, R. Site-controlled Ag nanocrystals grown by molecular beam epitaxy—Towards plasmonic integration technology. *J. Appl. Phys.* **112**, 124302 (2012).
- [10] Urbańczyk, A., Hamhuis, G. J. & Nötzel, R. Strain-driven alignment of In nanocrystals on InGaAs quantum dot arrays and coupled plasmon-quantum dot emission. *Appl. Phys. Lett.* **96**, 113101 (2010).
- [11] Leijnse, M. & Flensberg, K. Introduction to topological superconductivity and Majorana fermions. *Semicond. Sci. Technol.* **27**, 124003 (2012).
- [12] Beenakker, C. W. J. Search for Majorana Fermions in Superconductors. *Annu. Rev. Condens. Matter Phys.* **4**, 113–136 (2013).
- [13] Mourik, V. *et al.* Signatures of Majorana fermions in hybrid superconductor-semiconductor nanowire devices. *Science* **336**, 1003–7 (2012).

- [14] Oreg, Y., Refael, G. & von Oppen, F. Helical Liquids and Majorana Bound States in Quantum Wires. *Phys. Rev. Lett.* **105**, 177002 (2010).
- [15] Lutchyn, R. M., Sau, J. D. & Das Sarma, S. Majorana Fermions and a Topological Phase Transition in Semiconductor-Superconductor Heterostructures. *Phys. Rev. Lett.* **105**, 077001 (2010).
- [16] Urbańczyk, A., Hamhuis, G. J. & Nötzel, R. Single InGaAs Quantum Dot Coupling to the Plasmon Resonance of a Metal Nanocrystal. *Nanoscale Res. Lett.* **5**, 1926–1929 (2010).
- [17] Gibson, R. *et al.* Molecular beam epitaxy grown indium self-assembled plasmonic nanostructures. *J. Cryst. Growth* **425**, 307 (2015).
- [new1] Gehl, M. *et al.* Superconductivity in epitaxially grown self-assembled indium islands: progress towards hybrid superconductor/semiconductor optical sources. *JOSA B* **33** (7), C50-C56 (2016).
- [18] Grunthaner, P. J. Chemical depth profiles of the GaAs/native oxide interface. *J. Vac. Sci. Technol.* **17**, 1045 (1980).
- [19] Kim, J., Schoeller, H., Cho, J. & Park, S. Effect of Oxidation on Indium Solderability. *J. Electron. Mater.* **37**, 483–489 (2007).
- [20] Quitoriano, N. J. & Fitzgerald, E. A. Relaxed, high-quality InP on GaAs by using InGaAs and InGaP graded buffers to avoid phase separation. *J. Appl. Phys.* **102**, 033511 (2007).
- [new2] Bert, N. A. *et al.* In–Ga intermixing in low-temperature grown GaAs delta doped with In. *Appl. Phys. Lett.* **74**, 1442 (1999).
- [21] García, J. M. *et al.* Intermixing and shape changes during the formation of InAs self-assembled quantum dots. *Appl. Phys. Lett.* **71**, 2014 (1997).
- [22] Amrani, A., Djafari Rouhani, M. & Mraoufel, A. A Monte Carlo investigation of Gallium and Arsenic migration on GaAs(100) surface. *Appl. Nanosci.* **1**, 59–65 (2011).